Effective Physical Possesses on the Proton Beam Radiation in Water with Geant4 Simulation

Seyede Nasrin Hossenimotlagh[1*], Simin Avaz Zade[2], Abuzar Shakeri[3], Tahereh Mousavi[4], Jahangir Bayat[5]

[1,2,3,4,5]*Department of Physics, Azad Islamic University, Shiraz Branch, Iran, Shiraz*

Abstract

The aim of this work is description of quantitatively and qualitatively physical processes for proton therapy when proton pencil beam passing through water phantom. Therefore, at first, we determine absorbed dose with both of Maple programming and Geant4 simulation in suggested water phantom. Then, we used as CSDA method to calculate the proton range and range straggling. Also, with Highland formula the mean scattering angle is calculated and following it we investigate on the inelastic cross section, the ionization and excitation by protons in the inner and outer shells as well as charge transfer, stripping and ionization by neutral hydrogen. Finally, we estimate the probabilities of charge state and stopping cross section and straggling and fragmentation. The height, width, and depth of Bragg's peak are discussed through the investigation of collisions, processing, and random phenomena.

Key words: Bragg peak, proton therapy, radiotherapy, depth-dose, cross section.

1. Introduction

One of the most important types of cancer treatments to control cancer cells is radiotherapy. In the developed countries, every year about 20,000 cancerous patients are treated with high-energy X-rays photons [1]. Usually, radiotherapists use electron linear accelerators as sources of X-ray radiation. Despite this being so widely used, the absorbed dose actually reaches a maximum very rapidly after hitting the body and decreases slowly in an exponential manner. Thus, using X-rays is not an efficient way to reach the deep-seated tumors. In addition, not only at the entrance of the body, but also after the tumor, healthy tissues are irremediably damaged, as the photons traverse our organs. Treatment with proton beams is proven to be an effective way to cancer treatment. This method contributes to conventional forms of treatment such as chemotherapy, surgery, radiotherapy and X-ray. This article provides further information in this field. The use of proton therapy is the latest advancement in the treatment of various types of cancer. This method is a precise form of the beam therapy in which proton beam radiation on the cancer cells destroys them. When compared with the other conventional cancer treatments such as surgery, chemotherapy, and X-ray therapies, it achieves a high score in terms of accuracy and effectiveness. This method eliminates cancer cells without damaging healthy cells. Therefore, it significantly reduces the side effects of conventional cancer treatments. The use of this cancer treatment method was first introduced in 1954. Sinceو at the timeو there were few centers to treat cancer, it limited the use of this therapeutic approach. In this therapeutic approach, ionized particles or protons in the tumor are targeted. These protons generate and accelerate from a device called cyclotron (an accelerator that accelerates the charged particles after exiting the source by electric fields). The proton beam penetrates the body while at its lowest concentration. It reaches its highest concentration as soon as it enters the target cells. Protons have a relatively large mass and, consequently, do not become very scattered and focus only on the tumor. This radiation damaged the DNA of cancer cells without causing harm to the surrounding cells, while in the conventional therapeutic non-cancerous cells are damaged. Failure and DNA damage results in degradation of the cell's ability to divide or multiply, thereby affecting the growth of cancer cells. Cells can produce enzymes that repair damaged DNA, but cancer cells lose the ability to produce those enzymes. This leads to permanent damage to those cells and subsequently leads to annihilation them. Since adjuvant cells do not damage during treatment, they are significantly reduced the side effects compared to conventional treatments. The

duration of treatment depends on the size of the tumor from one to several weeks. If the treated tumor does not appear after five years, it is concluded that treatment has been successful .All of the rays with a certain energy have a certain range; very few protons penetrate more than this amount. Therefore, the dose transmitted to the tissue is maximized in the last few millimeters of the proton board. This peak is called Bragg, often known as SOBP. Determining the amount of proton energy during treatment can cause the most damage to cancer cells. Tissues that are closer to the surface of the body than the tumor will receive less radiation, so they will suffer less damage. Tissues that are more in depth than the tumor have very few protons, and their dosage is very low. In most cases, protons with different energies at different depths are used to eliminate all tumors. To confirm the effects of ionizing radiation it is important to know how its energy is distributed linearly. The linear energy transfer (LET) is a measure of the energy transferred to a matter per unit length as an ionizing particle travel through it. For photons, this indicates a poor distribution, but protons and other charged particles show a very different depth-dose curve. They generate Bragg's peak and a significant increase in stored energy in the very last region of their trajectory is observed, where they lose their entire energy and the deposited dose falls to zero. When protons pass through a matter, they experience Coulomb interactions with the orbiting electrons and nuclei of the atoms in the matter. Electrons may be released from the atomic shells and the atoms become ionized. The freed electrons damage the DNA of the cells and can sometimes ionize other neighboring atoms. As the electrons mass is small compared to that of protons, the protons lose in this process a very small amount of energy in a non-linear manner. In addition, protons may be involved in other inelastic processes, such as excitation of the matter or charge transfer. All these processes should be considered in detail to gain a precise knowledge about the behavior of proton beam in interaction with the patient body.

There are three types of proton-beam delivery methods: passive scattering, uniform scanning, and pencil beam scanning. When identifying treatment options and developing treatment plans, it is important to consider the method of proton-beam delivery. Pencil beam is the most modern form of delivering proton beams to patients. Pencil beam scanning does not require the use of patient-specific or field-specific devices (apertures, compensators) in the delivery of proton therapy treatment. This eliminates treatment delays, reduces treatment time, reduces costs, increases flexibility in treatment delivery, and reduces patient exposure to secondary radiation produced when the beam hits a device. Although it is claimed that proton therapy is very efficient, this is only true if the position and the dose can be calculated very accurately. The greatest advantage of proton therapy, which includes the concentration of the deposited energy on a small region of the space, may be lethal if there is even a very slight shift in the position of the Bragg peak. Despite the fact that it is possible to achieve the appropriate Bragg peak position through Monte Carlo-based simulator packages like GEANT4, the full understanding of the whole process is related to the height, width, and precise position of the depth-dose distribution requires analytical and/or semi-empirical models. This paper has been conducted on the physical processes involved in the transport of protons from the material in order to determine the precision in determining the Bragg peak position. We follow the same techniques used by Ding elder et al. [3] to determine the cross section for inelastic interactions of energetic protons in water phantom. Water phantom is a cubic with $100 \times 100 \times 100 cm^3$volume. These cross sections are used for determining the LET of ions in terms of the depth of their penetration according to the approach introduced by Obolensky et al. [4] and Surdutovich et al. [5]. Note that, in Refs. [4, 5], the main study is on carbon ions, but in this work, we focus on proton ions. In the current study, we analyze the different processes when a proton beam irradiated the water with two methods of Maple programing and Geant4 simulation [7]. Thus, the article is organized as follows. In section 2, we analyze the interaction of proton with matter. In section 3, shortly we familiar with Geant4 toolkit. In section 4, we study on the inelastic processes that contribute to the total cross section for protons passing through water phantom, and therefore, we follow the approach and use data in Refs. [3, 6] to calculate cross sections for different processes such as ionization, excitation, stripping and charge transfer. Also, the fragmentation of particle and processes like straggling, which determine the height and the width of the Bragg's peak are also described in this section. In Section 5, our numerical obtained results are described. Finally, we give a brief summary of our work.

2-Interaction of proton with matter

The mass stopping power as a function of traversed material is given by the Bethe-Bloch formula, [2]:

$$\frac{1}{\rho}\frac{dE}{dx} = Kz^2\frac{Z}{A}\frac{1}{\beta^2}\left[\frac{1}{2}\ln\frac{2m_e c^2\beta^2\gamma^2 T_{max}}{I^2} - \beta^2 - \frac{\delta(\beta\gamma)}{2}\right] \quad (1)$$

Where, z is the charge of the incident particle, Z and A are the atomic number and the mass number of the absorber, respectively. I is the mean excitation energy, $\delta(\beta\gamma)$,is the density effect correction to ionization energy loss, β and γ are the usual relativistic factors. T_{max} ,is the maximum of kinetic energy which can be imparted to a free electron in a single collision. It is important to note that the deposited energy is inversely proportional to the square of the velocity of the particle β. Upon entering the matter, the protons have maximum energy and therefore maximum velocity but as they traverse the matter they interact with the orbiting electrons, lose energy and velocity and deposit more and more dose. Physically, the dependence on v arises from the time needed for a Coulomb interaction to take place. If the particle moves faster, there is less time for the electric fields of the projectile and the atoms in the matter to interact, and thus less energy is deposited. The average energy deposited to the matter by radiation per unit mass of this matter is called the dose deposited by a ion beam, D:$D = 1.602 \times 10^{-10} \times \varphi \times \frac{dE}{\rho dx}(GY)$, where, $\frac{dE}{\rho dx}$ in $\frac{MeV.cm^2}{g}$is mass stopping power (see equation 1) and φ is the number of charged particles per cm^2.in this work $\varphi = 10^6 cm^{-2}$. In this work, we use the CSDA method to calculate the proton range. CSDA is calculated by integrating the initial and final energy of the incident particle on the inverse of the total stopping power, which is given by the: $CSDA\ R = \int_{E_f}^{E_0}\frac{dE}{S_{tot}}$In which $E_0$and E_f are the initial and final energy of the proton input at the target. The loss of energy of an ion in matter is a statistical process and it is not definite, and the Bethe equation yields only the average of energy lost. This change was first described by Bohr, who introduced the concept of energy regulation (σ_E): $\frac{d\sigma_E^2(x)}{dx} = K(x) - 2\frac{dS(E(x))}{dx}\sigma_E^2(x)$ where $K(x) = z^2\rho_e K\frac{1-\frac{1}{2}\beta^2}{1-\beta^2}$ .Therefore range straggling (σ_R) is defined as a function of energy from the solution of the $\frac{d\sigma_R^2}{dx} = \frac{1}{S(E)}\frac{d\sigma_E^2(x)}{dx}$ equation, where , S(E) is the total mass stopping power. Proton which passes through the matter may be deflected by the atomic nucleus, this process commonly referred to as scattering, or more precisely, a multiple coulomb scattering is observed, when angular scattering occurs due to the collective effect of many small single-scattering which are randomly happened. Both the proton and the nucleus are positively charged; therefore, their interactions are mostly Columbic. The Highland formula calculates the mean scattering angle θ_0: $\theta_0 = \frac{14.1MeV}{pv}z_p\sqrt{\frac{L}{L_R}}\left[1 + \frac{1}{9}\log_{10}\left(\frac{L}{L_R}\right)\right]rad$, where p is the proton momentum and v = βc is the proton velocity and L is the target thickness and L_R is the target radiation length. The length of the radiation is the distance that the energy of the radiation particles due to radiation losses decreases as much as the coefficient e^{-1} (≈ 0.37).

3-Geant4 simulation

The Geant4 code version 10.1.1 was used for this research. The physics lists adopted in this research were based on the suggestions from the user guide and recommended setting in other works [10, 11]. GEANT is a toolkit for the simulation of radiation transport in material. It suggests a set of physics models based on theoretical and experimental data. GEANT works based on a C++ program. The experimental set-up has to be explicitly described in the code, the primary particles have to be provided and the specific physics models to be used in the simulation should be included in the code. GEANT also represents some extra visualization tools.(for example, OpenGL, Wired, RayTracer, etc.).The materials and geometry part of the main is used to interpret the detector. The user has to form a concrete class from of the G4VUserDetectorConstruction abstract based on class. In the implicit method all the required materials, the detector geometry volume, and the classes of sensitive detector have to be made. The classes of sensitive detector should be set to the volumes of detector. The physics

part of the code is where the physics processes are selected and the particle interactions with matter are defined. Geant4 does not have any default particles or processes; it has to be explicitly defined within the code. A concrete class can be derived from the G4VUserPhysicsList abstract class. This concrete class should define all the required particles, all the required processes which should in turn be assigned to proper particles, and the cut-off ranges applied to the world. A step in Geant4 has two points and carries information such as the energy loss on the step and time-of-flight spent by the step of a particle. In case a step is limited by a volume boundary, the end point physically stands on the boundary and it logically belongs to the next volume. Since each step knows two volumes, boundary processes such as reflection and radiation of transition can be simulated. Geant4 tracking is general, it is independent of the particle type, and of the physics process related to a particle. While a process is being tracked in Geant4, it contributes to any possible changes in the physical quantities of the track. Each process can also create secondary particles and suggest variations in the state of the track. At the starting of a process, an event contains primary particles. To create the primary event, the concrete class has to be derived from the G4VUserPrimaryGeneratorAction abstract base class. A G4Event object is passed to one or more primary generator concrete class objects which generate primary vertices and primary particles. These primaries are pushed into a stack. When the stack is empty, the processing of an event is over. A G4Event class shows an event. Each event generates a primary vertices and particles list, hits collections, path collection, etc. This information is then sent to the run manager. In fact, a run is a collection of events which share the same detector conditions. A run in Geant4 is begun with the command 'BeamOn'. Within a run, the user cannot change the geometry of detector or the settings of the physics phenomena. At the starting of a run, the geometry is optimized for orientation, and cross-section tables are estimated in accordance with the materials given in the geometry. For visualization, user has to derive a concrete class from G4VVisManager in accordance with the computer environments. Geant4 creates interfaces such as RayTracer, WIRED, OPACS,OpenGL, DAWN and VRML to graphics drivers.

4 - Proton passage through water phantom

4.1. Inelastic cross section

In the beginning, we have studied the passage of a single proton through liquid water. When the energetic ion enters the matter, inelastic cross sections are typically small, but they grow to reach a maximum, namely the Bragg's peak, where the ion loses its energy at the highest rate. For our analysis, we follow mainly the approach from Ding elder et al. [3]. At the first we consider impact ionization, which is the dominant process contributing to the energy loss and resulting in the production of the secondary electrons, and then add several other terms, such as excitation, charge transfer, stripping and ionization by proton. The secondary electrons are not produced the process of arousal. The charge transfer phenomenon consists of the transfer of electrons from the water molecules to the projectile, which in the end are neutralized. When the projectile of a proton is discussed in this study, charge transfer involves the transfer of one single electron. The hydrogen atom formed can also ionize the matter or can become stripped, in which case it loses the previously absorbed electron.

4.1.1. Ionization by protons

The singly differentiated cross section, SDCS, is the basic quantity in the analysis of the ionization process. This shows total ionization cross section differentiated with respect to the energy, W, of the ejected electrons and is dependent on the kinetic energy of the projectile, T. We use a semi-empirical expression introduced by Rudd and co-workers [6], which was derived by adjusting the experimental data to Rutherford cross section, among other analytical models,

$$\frac{d\sigma(W,T)}{dW} = z^2 \sum_i \frac{4\pi {a_0}^2 N_i}{B_i}\left(\frac{R}{B_i}\right)^2 \times \frac{F_1(v_i) + F_2(v_i)\omega_i}{(1+\omega_i)^3\left(1+exp\left(\alpha(\omega_i - \omega_i^{max}/v_i)\right)\right)} \quad (2)$$

where the sum is taken over the five electron shells of the water molecule, $a_0 = /0529$ nm is the Bohr radius, R=13/6eV is the Rydberg constant, N_i is the shell occupancy, B_i is the ionization potential of the sub-shell i for water vapor, $\omega_i = W/B_i$ is the dimensionless normalized kinetic energy of the ejected electron. The dimensionless normalized velocity, v_i, is given by [5]

$$v_i = \sqrt{\frac{mV^2}{2B_i}} \tag{3}$$

where, m is the mass of the electron and V is the velocity of the projectile, which in the relativistic case is given by βC,
Also,

$$\beta = \sqrt{1 - \frac{1}{\gamma^2}} = \sqrt{1 - \left(\frac{Mc^2}{Mc^2 + T}\right)^2} \tag{4}$$

where, M is the mass of the projectile.

Eq. (3) uses the kinetic energy of an electron having the same velocity as the projectile, normalized by the corresponding binding energy. The expressions for the functions in Eq. (2) are

$$F_1(v) = A_1 \frac{ln(1+v^2)}{B_1/v^2 + v^2} + \frac{C_1 v^{D_1}}{1 + E_1 v^{D_1+4}} \tag{5}$$

$$F_2(v) = C_2 v^{D_2} \frac{A_2 v^2 + B_2}{C_2 v^{D_2+4} + A_2 v^2 + B_2} \tag{6}$$

$$W_i^{max} = 4{v_i}^2 - 2v_i - \frac{R}{4B_i} \tag{7}$$

Eqs. (5)–(7) show original non relativistic expressions for Rudd model. V^2 is calculated classically as a function of $2T/M$. The parameter set for the protons SDCS used in this work can be found in Table 1 and were calculated by Dingfelder and co-workers [3]. Surdutovich et al. [5] introduce some modifications on F_1 which account for the relativistic effects due to the high energies reached (up to $\beta \sim 0.6$),

$${F_1}^{rel}(v) = A_1 \frac{ln\left(1 + v^2/1 - \beta^2\right)}{B_1/v^2 + v^2} + \frac{C_1 v^{D_1}}{1 + E_1 v^{D_1+4}} \tag{8}$$

Table 1. Required parameters for the SDCS of protons on water (from Refs. [3,6]).

parameter	Outer shells		Inner shells
	Liquid	Vapor	K-shells
A_1	1.02	0.97	1.25
B_1	82.0	82.0	0.50
C_1	0.45	0.40	1.00
D_1	-0.80	-0.30	1.00
E_1	0.38	0.38	3.00
A_2	1.07	1.04	1.10
B_2	14.6	17.3	1.30
C_2	0.60	0.76	1.00
D_2	0.04	0.04	0.00
α	0.64	0.64	0.66

When we expand the Rudd's model to relativistic energies, we note that F_1 and F_2 tend to $A_1 \ln(v^2)/v^2$ and A_2/v^2, respectively. Since F_2 approaches zero faster, F_1 absorbs the relativistic corrections. This results from the fact that as $A_1 \sim A_2$, for high velocity($v \gg 1$), F_1 is always higher than F_2. In particular, the new ${F_1}^{rel}$ introduced by Surdutovich and co-workers [5] reproduces the same asymptotic behavior as Bethe-Bloch formula. In this work, the Rudd model with relativistic corrections has been employed to account for the ionization process. The parameter set for the SDCS of protons on water vapor is also given in 1992 by Rudd et al. [6] and are also shown on Table 1. The division into inner and outer shells that Rudd suggests for choosing one or another set of parameters has been accepted.
But we followed the approach from Ref. [3], which consists of separating the K-shell from the rest, as seen on Table 3. In their investigation, Rudd and co-workers reviewed the different approaches for the total cross sections and suggested this semi-empirical approach. According to Ref. [3], the latter does

not reproduce accurately the stopping cross section for liquid water due to the lack of a careful consideration of the water molecule's sub-shells. To overcome this, they suggest adding a partitioning factor G_j which adjusts the contributions of the sub-shells to the results from the Born approximation.

$$\frac{d\sigma}{dW} = \sum_{all\ j} G_j \frac{d\sigma^j}{dW_j} \tag{9}$$

In this work, we reproduce the previous expressions for liquid water from Ding elder et al. [3] directly, who obtained the parameter In this work, we reproduce the previous expressions for liquid water from Ding elder et al. [3] directly, who obtained the parameter set for liquid water by modifying the water vapor set until the equations reproduced the recommended ICRU stopping cross section for the desired material [8].

Table 2. Ionization energies (in eV) for the different sub-shells in the water vapor (B_j) and liquid water (I_j), the partitioning function G_j and the number of electrons N_j . The data are taken from Ref. [3].

Shell	Outer shells				Inner shells
	$\mathbf{2a_1}$	$\mathbf{1b_2}$	$\mathbf{3a_1}$	$\mathbf{1b_1}$	$\mathbf{1a_1}$
$\boldsymbol{I_j}$	32.30	16.05	13.39	10.79	539.00
$\boldsymbol{B_j}$	32.20	18.55	14.73	12.61	539.70
$\boldsymbol{G_j}$	0.52	1.11	1.11	0.99	1.00
$\boldsymbol{N_j}$	2	2	2	2	2

Table 3. required parameters for the excitation cross section for liquid water, taken from [3].

k	Excited state	$E_k(eV)$	a (eV)	J (eV)	Ω	v
1	$\tilde{A}^1B_1$	8.17	876	19820	0.85	1
2	$\tilde{B}^1A_1$	10.13	2084	23490	0.88	1
3	Ryd A+B	11.31	1373	27770	0.88	1
4	Ryd C+D	12.91	692	30830	0.78	1
5	Diffuse bands	14.50	900	33080	0.78	1

It must be noted that Rudd and co-workers developed their model for vapor water, and took the binding energies for this phase as parameters. Hence, even though our approach is for liquid water, the binding energies used in the SDCS (Eqs. (2), (3) and (7)) are those from water vapor. By integrating the SDCS over the secondary electron energy,W, the total cross section of impact ionization by the ion with kinetic energy T is obtained:

$$\sigma(T) = \int_0^{W_{max}} \frac{d\sigma(W,T)}{dW} dW \tag{10}$$

The maximum kinetic energy is

$$W_{max,i} = T - I_i \tag{11}$$

Note that in this case, the binding energy corresponds to that of liquid water.

4.1.2. Excitation by protons

For the case of excitation of the molecules of liquid water, we use a semi-empirical model which relates proton excitation cross section to electron excitation cross section, developed by Miller and Green [9]. The cross section for a single excitation of an electron in sub-shell k is given by the expression:

$$\sigma_{exc,k}(T) = \frac{\sigma_0 (Za)^{\Omega} (T - E_k)^{v}}{J^{\Omega+v} + T^{\Omega+v}} \tag{12}$$

where $\sigma_0 = 10^{-20}\ m^2$, $Z = 10$ is the number of electrons in the target material and E_k is the excitation energy for the state k. a ‹J ‹Ω and v are parameters (shown in Table 3), but they have physical meaning: a (eV) and Ω (dimensionless) represent the high energy limit and J (eV) and v (dimensionless) the low energy limit. We have taken the values recommended by Ding elder and his group, who in turn used the original suggestions in Ref. [9].

4.1.3. Charge transfer

There exists the possibility that an electron from the water joins the projectile, the proton in this case. A neutral hydrogen atom is then formed either in a bound state or in a state in which the electron travels with the proton at the same velocity. This phenomenon is known as charge transfer. Again, following Ding elder's approach [3], who showed the contribution of the charge-transfer cross section by an analytical formula:

$$\sigma_{10}(T) = 10^{Y(X)} \tag{13}$$

Where $X = \log T$ with T measured in eV and

$$Y(X) = [a_0 X + b_0 - c_0(X - x_0)^{d_0}\Theta(X - x_0)]\Theta(x_1 - X) + (a_1 X + b_1)\Theta(X - x_1) \tag{14}$$

Where $\Theta(X)$ the Heaviside step function and the other parameters is can be found in Table 4.

Table 4. required parameters for the charge transfer cross section, taken from [3].

a_0	b_0	c_0	d_0	a_1	b_1	x_0	x_1
-0.180	-18.22	0.215	3.550	-3.600	-1.997	-3.450	5.251

These parameters were obtained by considering the experimental data on water vapor [10–12] as a starting point and adjusting them to fit the contribution of the charge transfer to the total cross section in the recommended values for liquid water. The subscripts 10, in the charge transfer cross section means that the projectile goes from the state 1 to the state 0, where 1 corresponds to a proton and 0 to a neutral hydrogen.

Table 5. required parameters for the stripping total cross section, taken from [3].

A	B	C	D
2.835	0.310	2.100	0.760

4.1.4. Stripping of neutral hydrogen

The neutral hydrogen atom can undergo stripping or electron loss. As before, not many experimental data exist for liquid water. Hence, we decided to use a semi-empirical formula given by Rudd et al. [13] for the cross section. In this expression the harmonic mean of a low energy and a high energy part is considered. Parameters used are those obtained by Ding elder and his group to fit the recommended values for liquid water.

$$\sigma_{01}(T) = \left(\frac{1}{\sigma_{low}} + \frac{1}{\sigma_{high}}\right)^{-1} \tag{15}$$

The two parts of the stopping cross section may be calculated as

$$\sigma_{low}(T) = 4\pi {a_0}^2 C \left(\frac{\tau}{R}\right)^D \tag{16}$$

$$\sigma_{high}(T) = 4\pi {a_0}^2 \left(\frac{R}{\tau}\right)\left[A \ln\left(1 + \frac{\tau}{R}\right) + B\right] \tag{17}$$

Where A, B, C and D are fitted parameters as given by Table 5. R=13.6eV is the Rydberg constant and τ is the kinetic energy of an electron travelling at the same speed as the proton.

4.1.5. Ionization by neutral hydrogen

The last effect to be taken into account is the ionization by neutral hydrogen. Despite of the lack of direct experimental information on this process, Bolorizadeh and Rudd [14] concluded that the ratio of the SDCS for hydrogen impact to the SDCS for proton impact as a function of the energy of the secondary electron is independent on this parameter when the projectile energy is fixed.

We can then use the SDCS for protons as the starting point and correct it by a factor $g(T)$ that depends only on the particle energy $T(eV)$, that is:

$$\left(\frac{d\sigma}{dE}\right)_{hydrogen} = g(T)\left(\frac{d\sigma}{dE}\right)_{proton} \tag{18}$$

Where the correcting function is adjusted by Ding elder and his group to fit the values for liquid water provided by **ICRU 49** [8].

$$g(T) = 0.8(1 + exp\left[\frac{\log(T) - 4.2}{0.5}\right])^{-1} + 0.9 \tag{19}$$

4.2. From the total cross section to the LET

The total cross sections for the different processes considered above for protons in liquid water with charge transfer cross section is higher for low energies of the projectile but it falls to zero very fast for energies around 0.1MeV. It is then expected that only for low energies, the probability to find the projectile as a neutral hydrogen becomes important.

4.2.1. Probabilities of charge state and stopping cross section

The combination of the contributions to the total stopping cross section has to be done in such a way that it takes into account the state of the projectile. In the case of a proton, we have just considered two possible charge states: neutral hydrogen $(\mathrm{H}, \mathrm{i} = 0)$ and proton $(P, \mathrm{i} = 1)$. The total stopping cross section will be the sum over all charged states i of the particle [3],

$$\sigma_{st} = \sum_{i,j,i\neq j} \Phi_i\left(\sigma_{st,i} + \sigma_{ij}T_{ij}\right) \tag{20}$$

where the term T_{ij} denotes the energy loss in the charge changing process, from state i to state j. Only one electron will be ripped out from the water molecule in the charge transfer process, and so we can suppose the most probable sub-shell to undergo the reaction is that with the smallest binding energy. This way we can establish a lower bound for the sum $T_{01} + T_{10}$ as the ionization energy of water I_0 plus the kinetic energy of the electron,

$$T_{01} + T_{10} = I_0 + \frac{mv^2}{2} \tag{21}$$

and Φ_i is the probability that the projectile is in state i. This is determined by the charge transfer and the stripping cross section:

$$\Phi_0 = \frac{\sigma_{10}}{\sigma_{01} + \sigma_{10}} \tag{22}$$

$$\Phi_1 = \frac{\sigma_{01}}{\sigma_{01} + \sigma_{10}} \tag{23}$$

Eq. (20) may now be rewritten as

$$\sigma_{st} = \Phi_0\sigma_{st,0} + \Phi_1\sigma_{st,1} + \sigma_{st,CC} \tag{24}$$

$$\sigma_{st,CC} = \frac{\sigma_{01}\sigma_{10}}{\sigma_{01} + \sigma_{10}}(I_0 + \tau) \tag{25}$$

The stopping cross sections are calculated as

$$\sigma_{st,i} = \int_0^{E_{max}} E \frac{d\sigma_i(E,T)}{dE} dE \quad (26)$$

where E_{max} is the maximum energy loss by the projectile in the corresponding inelastic process.The total stopping cross section is compared with the PSTAR values [15]. The reference data base for stopping power and range tables for protons (PSTAR) is provided by the National Institute of Standard and Technology (NIST) of the US department of Commerce. These values are obtained, for high energies, through Bethe's stopping formula including shell corrections, Barks and Bloch corrections [16, 17] and density effect corrections. The mean excitation energy, I, used in PSTAR is taken from ICRU 37 [18], corresponding to $I = 75eV$ for liquid water. For low energies, experimental data in PSTAR are fitted to empirical formulas. By definition, the linear energy transfer is proportional to the stopping cross section

$$\frac{dT}{dx} = -n\sigma_{st}(T) \quad (27)$$

where $n = 3.343 \times 10^{28} molecules/m^3$is the number density of water molecules. The position of the projectile as a function of its kinetic energy is obtained by integrating the inverse of LET [4, 5]

$$x(T) = \int_T^{T_0} \frac{d\acute{T}}{\left|d\acute{T}/d\acute{x}\right|} \quad (28)$$

where T_0 is the initial energy of the projectile. The parametric representation of LET versus depth is known as the depth-dose distribution. This process, used to calculate the energy transfer, is known as Continuous Slowing Down Approximation (CSDA). In this approximation, the projectile is assumed to lose energy in a continuous way. However, energy loss by a proton is a stochastic process, which produces variations in the range of the particles. In addition, the projectile might react with a water molecule and become fragmented. Then, for a real model we need to include two important contributions: straggling and nuclear fragmentation.

4.2.2. Straggling and fragmentation

Straggling accounts for the stochastic fluctuations in the range of the particles which traverse the medium. The straggling model considered here claims that the ranges of the projectiles follow a Gaussian distribution. The so-called broad-beam depth-dose curve results from the convolution of the previously CSDA LET with this Gaussian range straggling distribution. The concept is known as ''depth scaling'' and was introduced by Carlson et al. [19]. For each point x in the trajectory, it is assumed that every particle in the beam has an effective penetrated depth $\acute{x}$. These effective depths are distributed as a Gaussian centered on the actual penetrated depth x, which coincides with the CSDA range

$$\pi(x,\acute{x}) = \frac{1}{\sqrt{2\pi}\sigma_{strag}(x)} \exp\left(-\frac{(\acute{x}-x)^2}{2{\sigma_{strag}}^2(x)}\right) \quad (29)$$

where σ_{strag} is the variance, which may be obtained from a phenomenological formula given by Chu et al. [20] and depends in general on x. Nevertheless, the shape of the depth-dose distribution allows us to assume that it is approximately constant, with $\sigma(x) \sim \sigma(R_0)$ [21], since most of the curve is approximately flat and will not be significantly affected by the convolution. The expression for $\sigma_{strag}(x)$ is then

$$\sigma_{strag}(x) = 0.012x^{0.951}A^{-0.5} \quad (30)$$

where A denotes the ion's mass number [21]. Straggling has two important consequences on the depth-dose distribution. Firstly, as fewer particles arrive to the same final position, the dose in the peak is considerably reduced.

In addition, different particles have different ranges, and thus the peak is broadened. Nuclear fragmentation accounts for the possibility that when the projectile hits a target, it undergoes fragmentation. Two different effects need to be considered. The first one is the reduction of the beam

fluency, lowering the height of the depth-dose distribution at the peak. On the other hand, fragments can be produced in the same direction of the original beam. If lighter elements are formed, as having a longer range, they produce a tail in the depth-dose distribution which goes clearly beyond the position of the Bragg peak maxima. For protons, fragments are not important and so a tail is not observed. Hence, in this work we only include fragmentation by considering the reduction in the number of particles of the beam N. This model deals with a pencil beam with a single projectile, so the concept of fluency loses its meaning within this context (it would be a Dirac delta function). Instead, the fragmentation effect is considered through the decay of the total number of particles. If the projectile has probability P to react with a water nucleus, then:

$$\frac{dN(x)}{dx} = -PN(x) \tag{31}$$

$$N(x) = N_0 e^{-Px} = N_0 e^{-x/\lambda} \tag{32}$$

where λ is called mean free path length and N_0 is the initial number of incident protons. From the prediction of Ref. [22], we have $\lambda = 435\ mm$, for protons in liquid water. The broad-beam depth-dose curve considering fragmentation and straggling is therefore calculated as

$$\langle \frac{dT}{dx}(x) \rangle = N(x) \int_0^{R_0} \pi(x, \acute{x}) \frac{dT}{d\acute{x}} d\acute{x} \tag{33}$$

There is one additional process which has not been considered, multiple scattering, which accounts for the divergence of the beam as it travels along the matter. It has been shown that multiple scattering produces changes on the shape of the Bragg peak [23], especially on the amplitude and the peak to entrance dose ratio, although not on the range. Usually, hadron therapy simulations merely apply normalization procedures to fit the experimental data [24], as the effect is only due to a reduction of the fraction of primary particles. To compare with experimental data, the current model normalizes the depth-dose distribution to the experimental entrance dose and so scattering is not included.

5. Results and discussion

GEANT4 provides data on the depth-dose distribution of protons in water phantom. In Figs .1a and b the two and three dimensional variations of deposited absorbed dose in terms of proton energy and penetration depth in water phantom by applying equ.1 using Maple programing and Geant4 simulation are shown, respectively. By comparing the Figs.1a and b, we find that the theoretical and Geant4 simulation methods are consistent with each other numerically, also in Figs.1,it is seen that the height and width of Bragg's peaks with increasing proton energy and depth penetration are changed and with increasing the proton energy the height of Bragg's peak is decreased. As we have already mentioned, highly energetic protons have a lower probability to interact with the matter and hence the energy per unit length they deposit is also lower. When their energy decreases the linear energy transfer increases considerably. They lose their whole remaining energy in a short distance. In this way, the final range of the projectile is mostly determined by the distance traveled before reaching the threshold. In the Bethe-Bloch equation, ionization and arousal are shown by the projectile, and these cases only play a role in the energy of more than 1MeV.

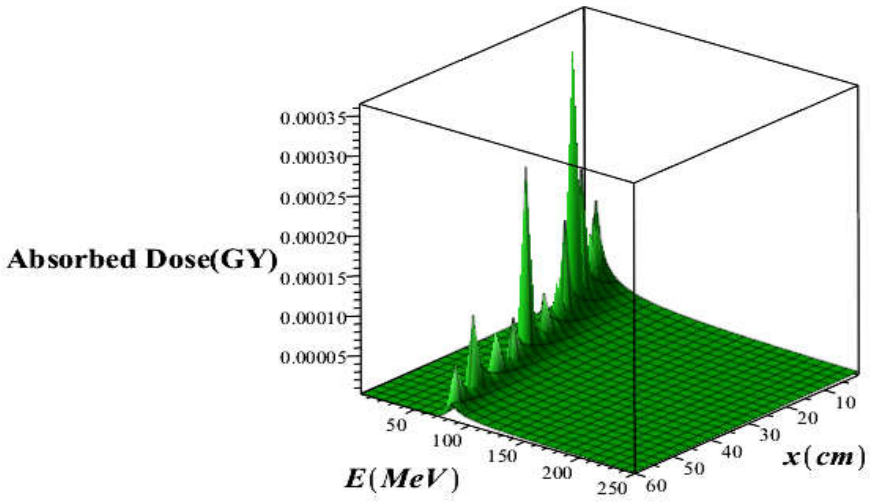

a)

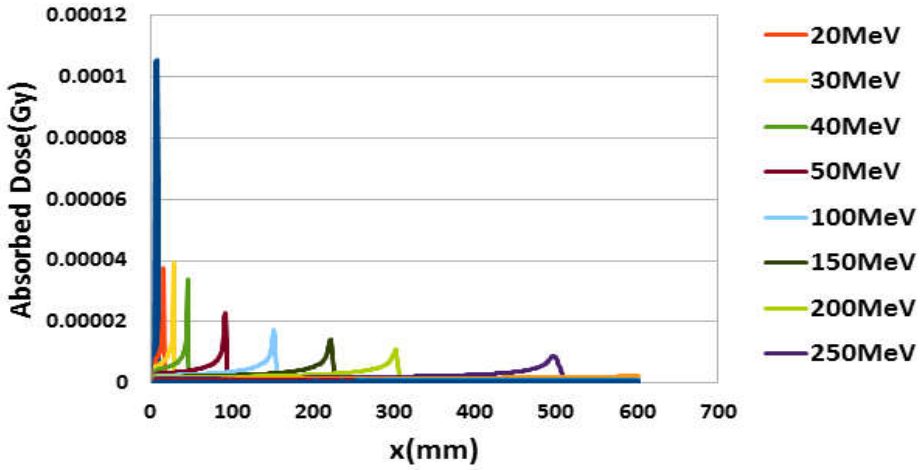

b)

Figure1: a) Three and b) Two dimensional of absorbed dose in terms of depth penetration for different proton energy using Geant4 simulation and maple programming, respectively in water phantom

In Figs.2a, b and c variations of CSDA R, straggling range and mean scattering angle of proton in water phantom using Geant4 simulation as a function of proton energy are shown, respectively.

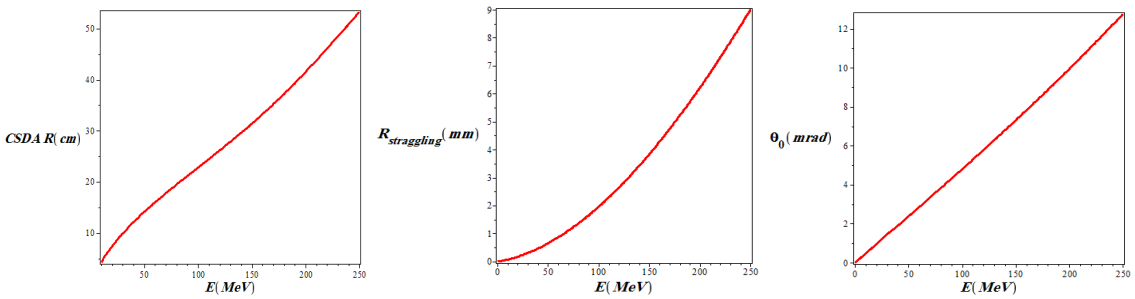

a) b) c)

Figure2: Variations of a) CSDA R b) straggling range c) mean scattering angle of proton in water phantom using Geant4 simulation as a function of proton energy

In Fig.3.a, the behavior of dimensionless normalized velocity (v_i) versus the ionization potential of the sub-shell i (B_i) and the kinetic energy of the projectile (T) for water vapor is plotted. For better understanding Fig. 3a., we plotted Figs.3b and c, and Figs.4. From Fig. 3b, we find that with increasing T both B_i and dimensionless normalized velocity (v_i) increases. But in Figs.4, we see that v is zero at T = 0, but in $T = 100\ and\ 250MeV$, with increasing B_i the v_i parameter nonlinearly decreases.

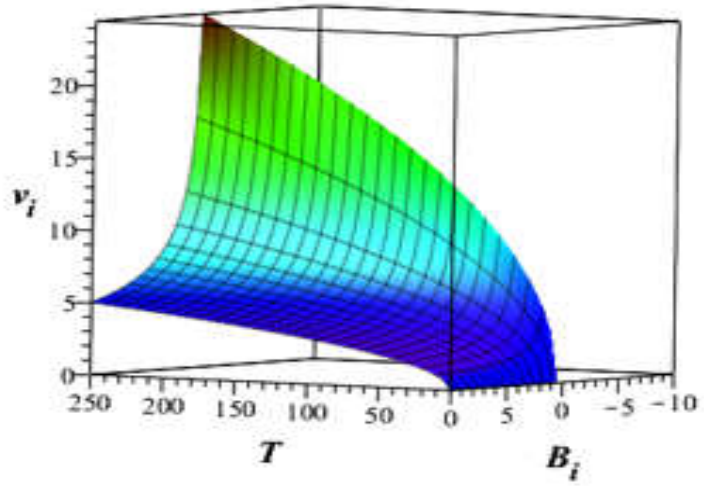

a)

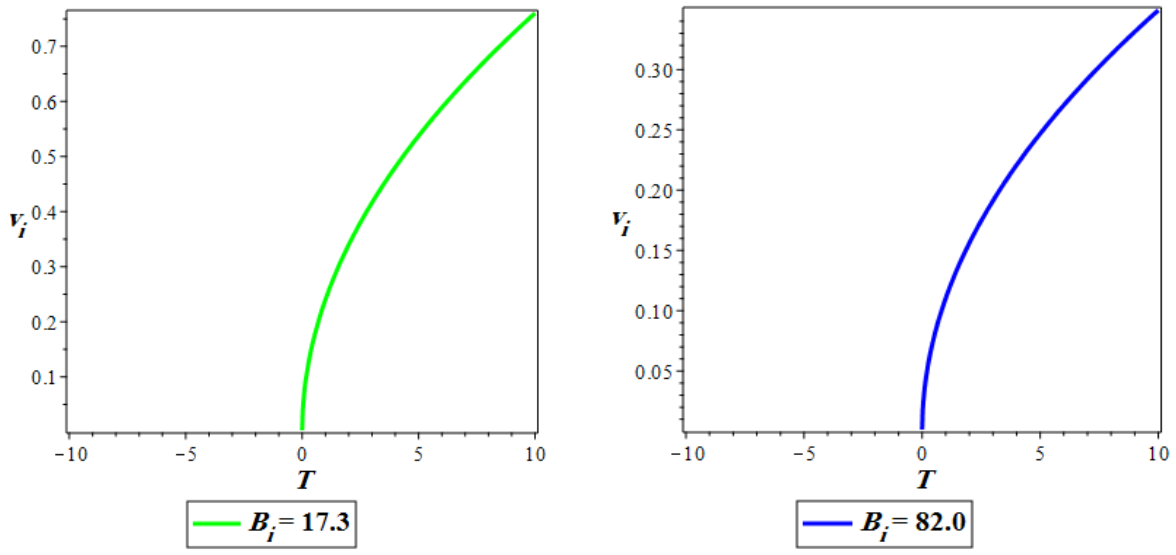

b) c)

Figure 3: a) Three b) two c) two dimensional variations of dimensionless normalized velocity (v_i) versus the ionization potential of the sub-shell i (B_i) and the kinetic energy of the projectile (T) for water vapor.

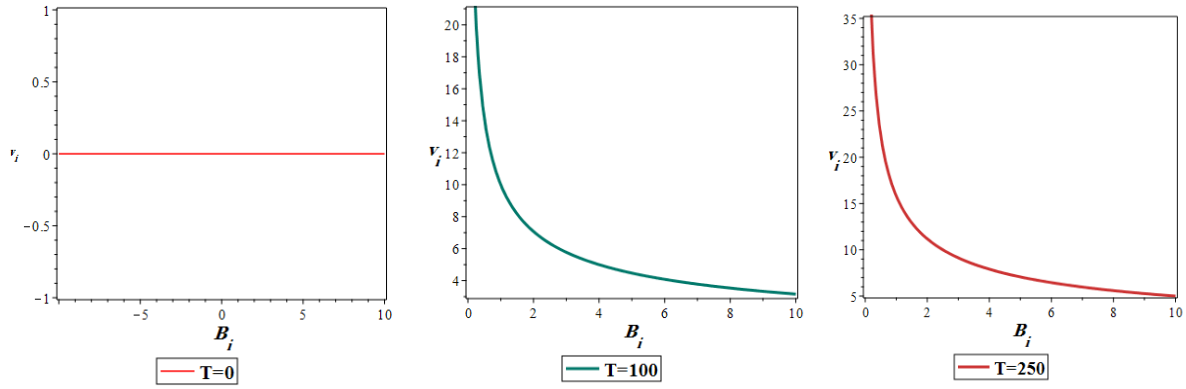

Figure 4. Variations of dimensionless normalized velocity (v_i) versus the ionization potential of the sub-shell i for water vapor (B_i) in different kinetic energy of the projectile (T in MeV)

Fig.5, shows that the β parameter is a function of T and with increasing T this parameter is increased nonlinearly.

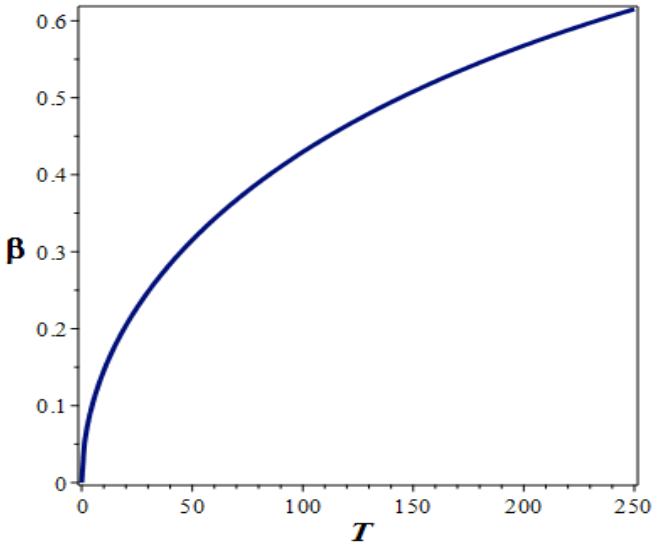

Figure 5. Variations of β versus the kinetic energy of the projectile (T in MeV)

Then in Fig.6 we plotted the functions of $F_1(v)$ and $F_2(v)$ versus v in the different three modes according to Table 1. From it we find that with increasing v (for liquid and vapor water) both states of outer shells nonlinearly decreases but inner shells state increases, while $F_2(v)$ has the opposite behavior.

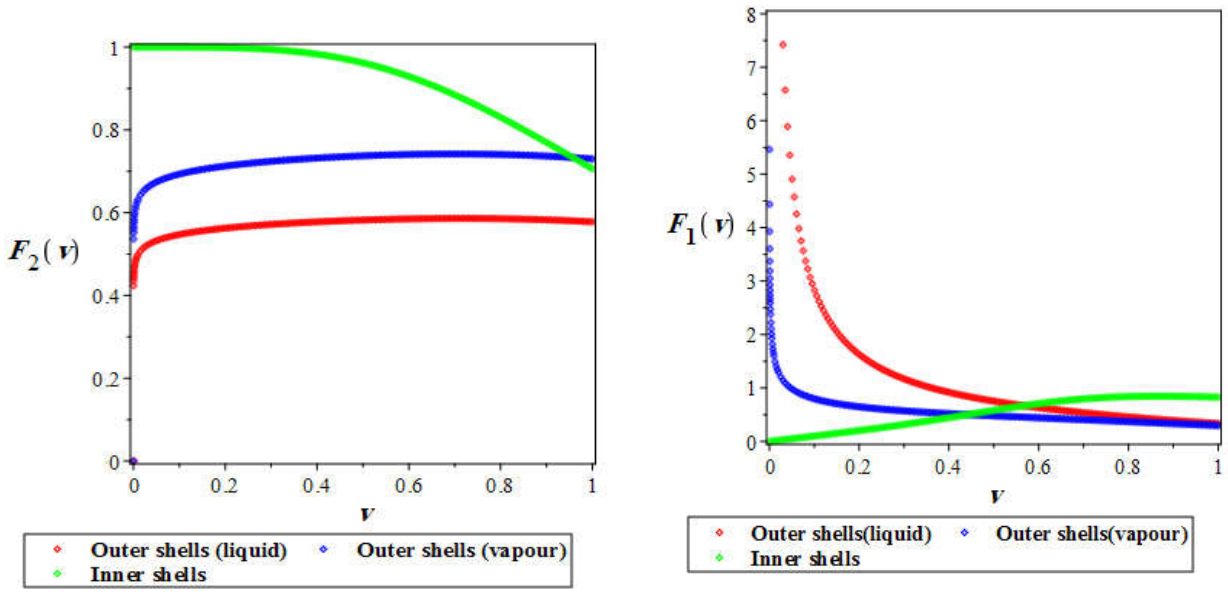

Figure 6. Variations of $F_1(v)$ and $F_2(v)$ versus v for different three modes using Table 1.

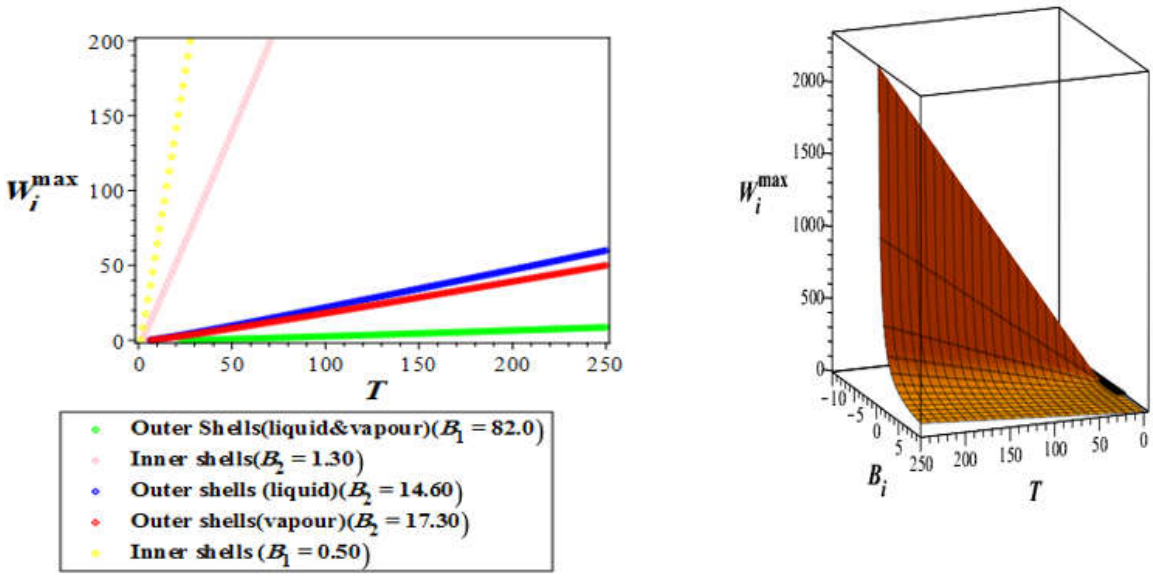

Figure 7. Two- and three-dimensional variations of $W_i{}^{max}$ versus the kinetic energy of the projectile (T) for different five modes of ionization potential of the sub-shell i for water vapor (B_i) using Table 1.

In Fig. 7, it is seen that $W_i{}^{max}$ is linearly increased with increasing kinetic energy (T)for five states which is expressed according to Table 1. Fig. 8 shows the variations of cross section for a single excitation of an electron $\left(\sigma_{exc,k}(T)\right)$ versus kinetic energy (T) for the different sub-shell k .According to this Fig. the outer shell for both of liquid and vapor water decreases with increasing v but for inner shell this result is inversed.

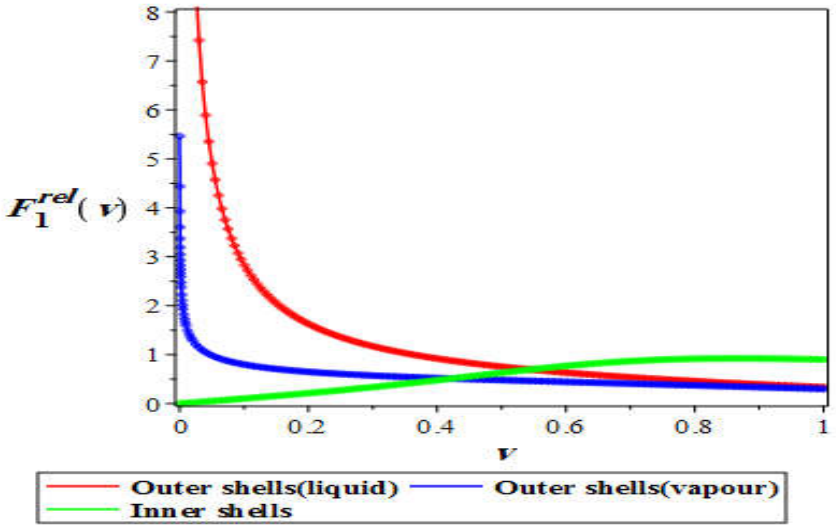

Figure 8. Variations of $F_1{}^{rel}(v)$ *versus v for different three modes using Table 1.*

Afterward in Fig.9, we investigated the variations of cross section for a single excitation of an electron $\left(\sigma_{exc,k}(T)\right)$ versus kinetic energy (T) for the different sub-shell k,it is seen that for $k = 1$ with increasing kinetic energy (T) cross-section for a single excitation of an electron is equal to zero and for $k = 2$ up to $T = 45MeV$ is equal to zero and then extends nonlinearly from 45 onwards. But for $k = 3, 4\ and\ 5$, at first it decreases and then increases.

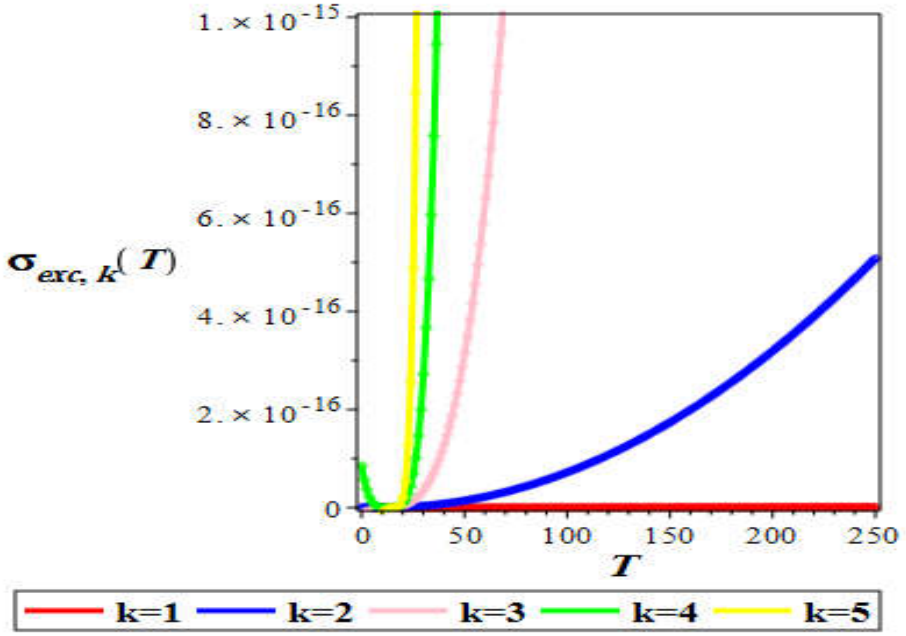

Figure 9. Variations of cross section for a single excitation of an electron $\left(\sigma_{exc,k}(T) in\ barn\right)$ versus kinetic energy ($T\ in\ MeV$) for the different sub-shell k.

Then in Fig. 10, charge transfer cross section from 0 to one and two parts of the stopping cross section with increasing kinetic energy (T) increase, but charge transfer cross section from 1 to 0 decreases nonlinearly.

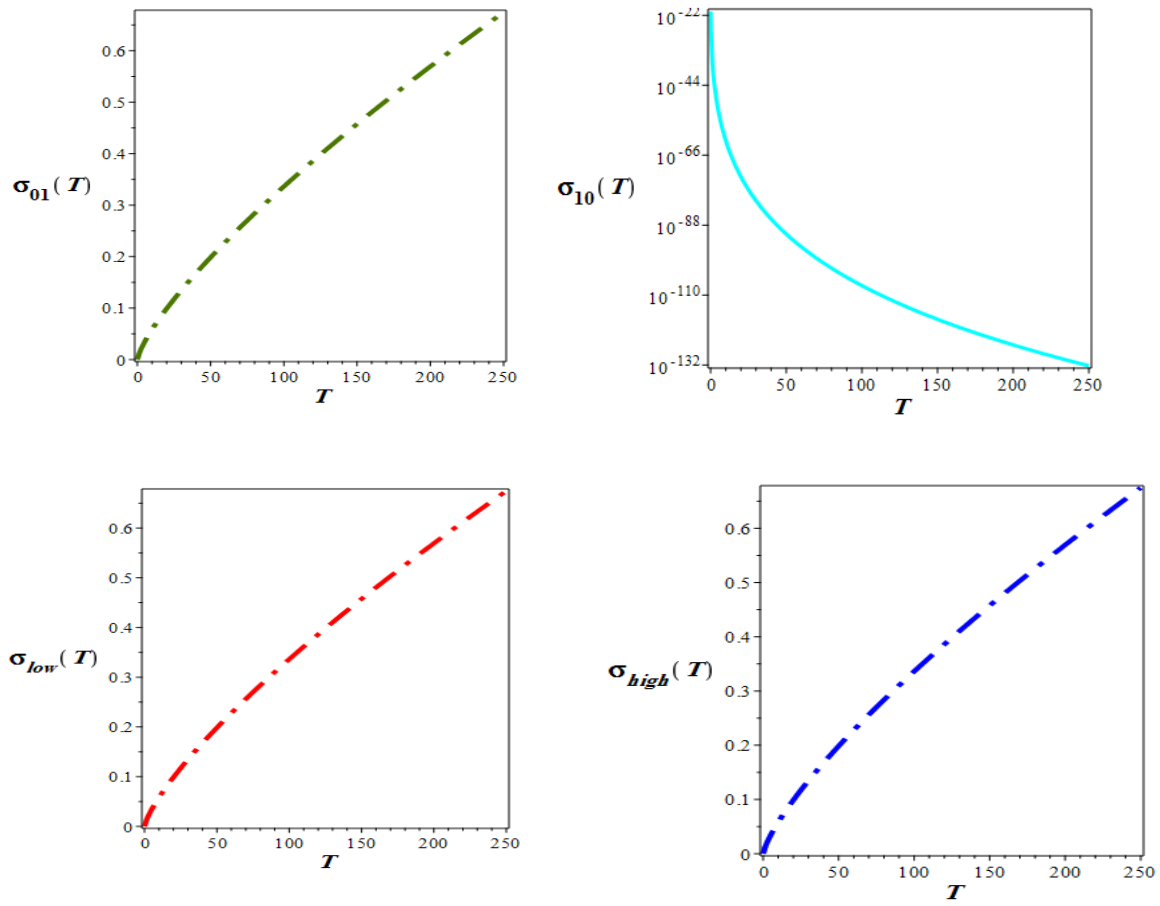

Figure 10. Variations of charge transfer cross section from 1 to zero and from zero to one and two parts of the stopping cross section versus of kinetic energy using tables 4 and 5.

In Fig. 11, we investigated the probability of an object being placed in two positions, one and zero, of the cross section and the stopping cross section in both states versus kinetic energy. $\Phi_1$is fixed in 1, but Φ_0, σ_{st} and $\sigma_{st,CC}$ with increasing kinetic energy (T) decreases.

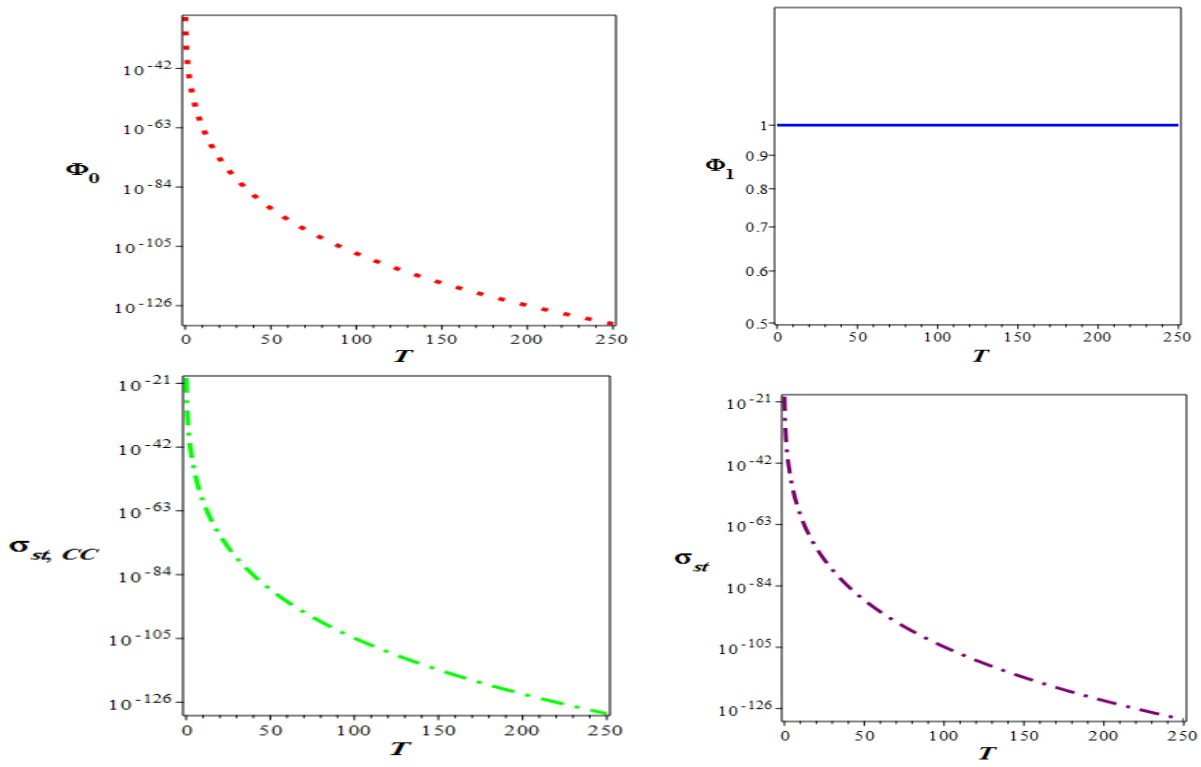

Figure 11. The probability of an object being placed in two positions, one and zero, of the cross section and the stopping cross section in both states versus kinetic energy.

In Fig. 12, variations of linear energy transfer versus proton energy is given, which is increased nonlinearly with increasing T.

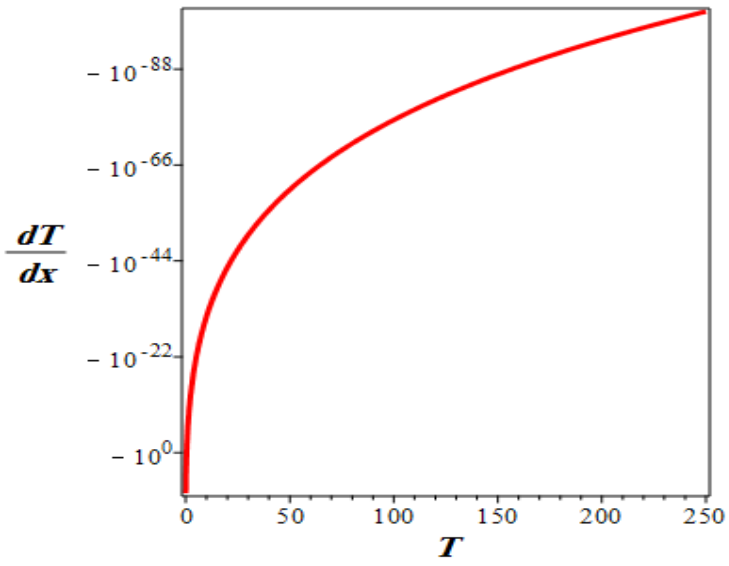

Figure 12. Variations of linear energy transfer proportional to the stopping cross section versus kinetic energy

In the end, in Fig. 13, we plotted the 2 and 3 dimensional variations of effective depths versus the actually penetrated depth x and effective penetrated depth $\acute{x}$, we found that in each selected $\acute{x}$ effective depths $\pi(x, \acute{x})$has one peak.

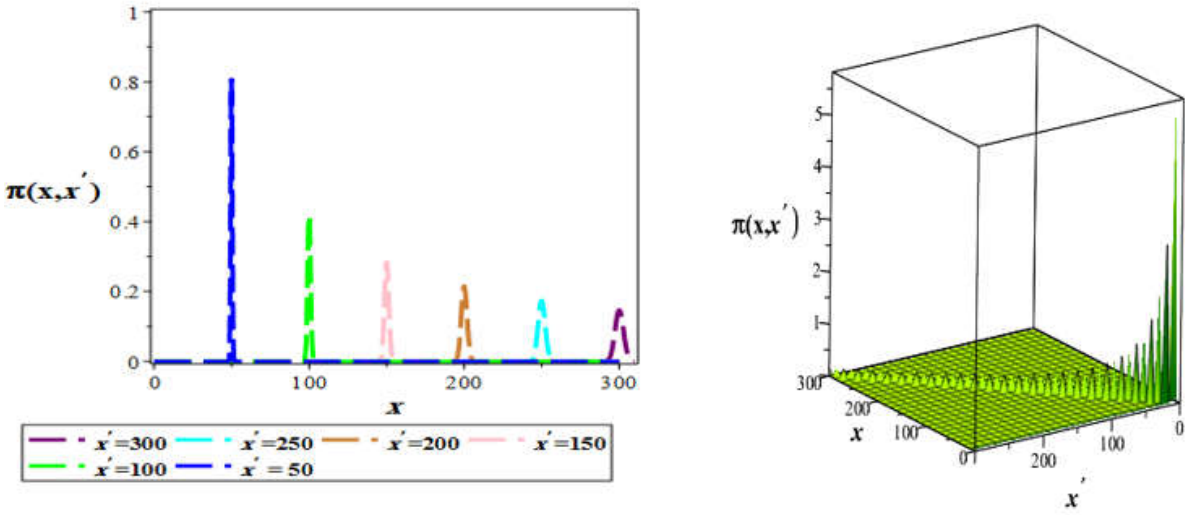

Figure 13. Variations of effective depth versus the actually penetrated depth x and effective penetrated depth $\acute{x}$

Bortfeld [26] shows that the relation between the range,R_0, and the initial kinetic energy of the projectile, T_0, is given by:

$$R_0 = \alpha T_0^P \qquad (34)$$

Where, $\alpha = 0.022\ mmMeV$ and P is approximately 1.77 for the energy range of 70–250MeV. Fig. 14 shows the range of protons in liquid water for different initial kinetic energies using Eq. (34)

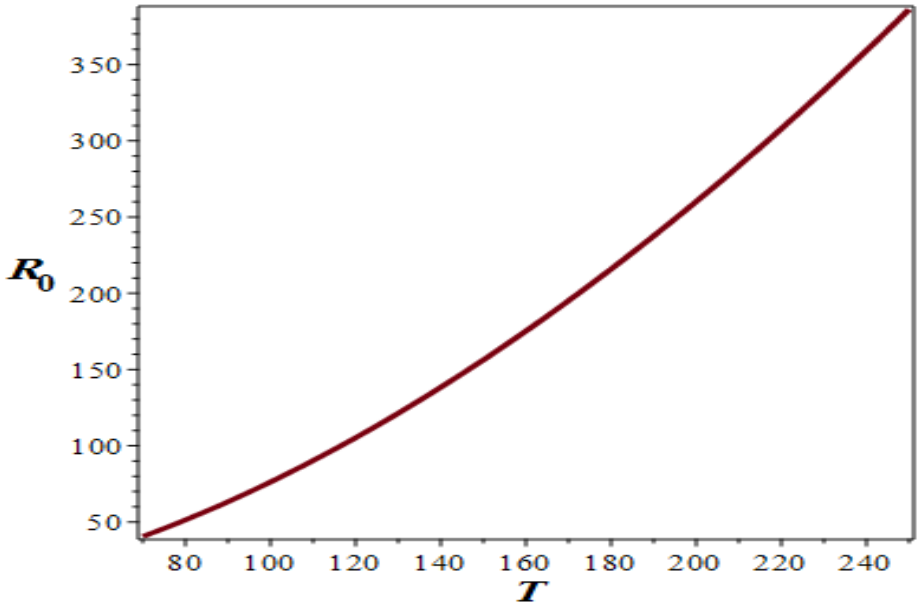

Figure 14. $R_0(\ in\ mm)$ Variations as a function of T (in MeV) in water

If we compared this range with given range from Geant4 simulation (Fig.2) and also with calculated range using the semi-empirical model and the Bethe-Bloch formula in Ref. [26], are in approximately agreement in the energy range of 70–250MeV, but the estimated range from Geant4 simulation in this work is more precise.

Eq. (34) is constructed so as to fit the experimental results. We observe that a great agreement for the range of protons in liquid water. We have therefore obtained an explanation for the passage of protons through the matter which reproduces accurately the results from Monte Carlo simulations. In order to further address the physics behind the Bragg peak features, we now analyze the individual contribution of the different inelastic processes to the depth-dose curve. For a typical proton beam with initial kinetic energy of 100 MeV, it is observed that if we neglect stripping, charge transfer and also hydrogen ionization terms, the change produced in the position of the peak is lower than 1 mm; a negligible distance. In addition, the linear energy transfer deposited in the peak is reduced around 0.005%. If only the excitation term is removed and the other contributions are all kept, we observe a shift in the position of the peak of around 1.5 mm, whereas, the change in the amount of energy deposited per unit length is negligible. Finally, removing just proton ionization makes the Bragg peak vanish. This shows that, from all the physical processes taking place in this situation, only proton ionization and excitation (the latter in a smaller scale) contribute to the properties of the Bragg peak. Thus, the other terms, affecting only low energies, produce all together solely a very small variation in the height and width of the peak.

6. Summary

In proton radiotherapy, protons interact with matter in three ways: i) Multiple collisions with atomic electrons cause them to lose energy and eventually stop. ii) Multiple collisions with atomic nuclei cause them to scatter by a few degrees. iii) Occasional hard scatters by nuclei or their constituents throw dose out to large distances from the beam. Unlike the first two processes, these hard scatters or 'nuclear interactions' do not obey any simple theory, but they are rare enough to be treated as a correction. All three interactions combine in the Bragg curve, the depth-dose distribution of a mono-energetic beam stopping in water and the signature property of charged radiotherapy beams. In this research, for the first time we have considered comprehensive physical processes in detail that can affect on the proton beam radiation in water that can be help the cancer treatment. Using these different processes, we can determine the absorbed dose deposited, the different effects contributing to total stopping cross section including ionization and excitation of the medium, charge transfer, stripping and ionization by the neutral projectile in water phantom. Our obtained results show that, since straggling dominates the Bragg peak, and is a constant fraction of range, it follows that Bragg peaks taken at lower energies are sharper.

References

[1] U. Amaldi, G. Kraft, Radiotherapy with beams of carbon ions, Rep. Prog. Phys. 68 (2005) 1861–1882.

[2] D.E. Groom, S.R. Klein, Passage of particles through matter, Eur. Phys. J. C 15 (1- 4) (2000) 163–173.

[3] M. Dingfelder, M. Inokuti, H.G. Paretzke, Inelastic-collision cross sections of liquid water for interactions of energetic protons, Radiat. Phys. Chem. 59 (2000) 255–275.

[4] O.I. Obolensky, E. Surdutovich, I. Pshenichnov, I. Mishustin, A.V. Solov'Yov, W. Greiner, Ion beam cancer therapy: fundamental aspects of the problem, Nucl. Instr. Meth. B 266 (2008) 1623–1628.

[5] E. Surdutovich, O.I. Obolensky, E. Scifoni, I. Pshenichnov, I. Mishustin, A.V. Solov'yov, W. Greiner, Ion-induced electron production in tissue-like media and DNA damage mechanisms, Eur. Phys. J. D 51 (2009) 63–71.

[6] M.E. Rudd, Y.K. Kim, D.H. Madison, T.J. Gay, Electron production in proton collisions with atoms and molecules: energy distributions, Rev. Mod. Phys. 64 (1992) 441–490.

[7] S. Agostinelly et al., Geant4: a simulation toolkit, Nucl. Instr. Meth. A 506 (2003) 250–303.

[8] Stopping Power and Ranges for Protons and Alpha Particles, ICRU Report No. 49 (1993).

[9] J.H. Miller, A.E.S. Green, Proton energy degradation in water vapor, Radiat. Res. 54 (1973) 343–363.

[10] B.G. Lindsay, D.R. Sieglaff, K.A. Smith, R.F. Stebbings, Charge transfer of 0.5, 1.5and 5 KeV protons with H2O: absolute differential and integral cross sections,Phys. Rev. A 55 (1997) 3945–3946.

[11] R. Dagnac, D. Blanc, D. Molina, A study on the collision of hydrogen ions H1 , H2 and H3 with a water–vapour target, J. Phys. B 3 (1970) 1239 1251.

[12] L.H. Toburen, M.Y. Nakai, R.A. Langley, Measurement of high-energy chargetransfer cross sections for incident protons and atomic hydrogen in various gases, Phys. Rev. 171 (1968) 114–122.

[13] M.E. Rudd, Y.K. Kim, D.H. Madison, J.W. Gallagher, Electron production in proton collisions with atoms and molecules: total cross sections, Rev. Mod. Phys. 57 (1985) 965–994.

[14] M.A. Bolorizadeh, M.E. Rudd, Angular and energy dependence of cross sections for ejection of electrons from water vapor II. 15–150 KeV proton impact, Phys. Rev. A 33 (1986) 888–892.

[15] http://physics.nist.gov/PhysRefData/Star/Text/PSTAR.html.

[16] L.E. Porter, The Barkas-effect correction to Bethe-Bloch stopping power, Adv. Quantum Chem. 46 (2) (2004) 91–119.

[17] V.A. Khodyreva, On the origin of the Bloch correction in stopping, J. Phys. B: At. Mol. Opt. Phys. 33 (22) (2000) 5045–5056.

[18] Stopping Powers for Electrons and Positrons, ICRU Report No. 37 (1984).

[19] A.K. Carlsson, P. Andreo, A. Brahme, Monte Carlo and analytical calculation of proton pencil beams for computerized treatment plan optimization, Phys. Med. Biol. 42 (1997) 1033–1053.

[20] W.T. Chu, B.A. Ludewigt, T.R. Renner, Instrumentation for treatment of cancer using proton and light-ion beams, Rev. Sci. Instr. 64 (1993) 2055–2122.

[21] P. Kundrat, A semi-analytical radiobiological model may assist treatment planning in light ion radiotherapy, Phys. Med. Biol. 52 (2007) 6813–6830.

[22] L. Sihver, C.H. Tsao, R. Silberberg, T. Kanai, A.F. Barghouty, Total reaction and partial cross section calculations in proton-nucleus (Zt < 26) and nucleusnucleus reactions (Zp and Zt < 26), Phys. Rev. C 47 (3) (1993) 1225–1236.

[23] A.J. Wroe, I. Cornelius, A. Rosenfeld, The role of nonelastic reactions in absorbed dose distributions from therapeutic proton beams in different medium, Med. Phys. 32 (1) (2005) 7–41.

[24] A. Lechner, P. Maria Grazia, Analysis of Geant4 simulations of proton depth dose profiles for radiotherapy applications, in: IEEE Nuclear Science Symposium, Dresden (2008).

[25] P. Sigmund, A. Schinner, H. Paul, Errata and Addenda for ICRU Report 73, Stopping of Ions Heavier than Helium International Commission on RadiationUnits and Measurements (2009).

[26] T. Bortfeld, An analytical approximation of the Bragg curve for therapeutic proton beams, Med. Phys. 24 (1997) 2024–2033.